The Journal of Green Energy and Environmental Engineering

Research Paper

Adsorption of tetracycline in water by Fe^{3+} functionalized carboxymethyl chitosan aerogel

Ignacio Abad[1], Logan Leibfarth[2,*]

[1] Department of Civil and Environmental Engineering and Construction, University of Nevada, Las Vegas, NV, USA
[2] The Molecular Foundry, Lawrence Berkeley National Laboratory, Berkeley, California 94720, United States
*Corresponding author: Long.Leibfarth@lbl.gov

Abstract. Using carboxymethyl chitosan (CMCS) as raw material, Fe^{3+}-initiated gelation successfully produced a novel CMCS@Fe^{3+} composite aerogel for tetracycline (TC) adsorption. The study demonstrates that this composite exhibits outstanding adsorption performance for TC. At 298 K, the maximum adsorption capacity fitted by the Sips model isotherm is as high as 785.85 mg/g, significantly exceeding most previously reported data. Material characterization, density functional theory (DFT) calculations, and material ratio experiments revealed synergistic effects between CMCS and Fe^{3+} during adsorption. Hydrogen bonding and Fe^{3+} coordination were identified as key adsorption mechanisms, with Fe^{3+} coordination playing a central role. Furthermore, this adsorbent demonstrated stable performance in cyclic adsorption experiments, achieving satisfactory adsorption results even under varying inorganic salt concentrations and simulated aquaculture wastewater treatment scenarios. In summary, CMCS@Fe^{3+} exhibits significant application potential for tetracycline removal from water.

Keywords: *Microplastic dissolved organic matter (MPDOM); Light degradation; Spectral analysis; Fourier transform infrared spectrum; Mass disparity network analysis*

Received on 15 Feb 2025, Accepted on 15 April 2025, Published on 15 May 2025

1 Introduction

Tetracycline-class antimicrobials represent a group of broad-spectrum bacteriostatic agents, frequently incorporated into livestock feed formulations for prophylactic and therapeutic management of diverse veterinary pathologies. In China, the use of tetracyclines among various veterinary antimicrobials is particularly prominent, accounting for as high as 40.5% [3]. Most of the unused antibiotics enter the environment through various pathways such as excretion from humans and animals after medication and medical waste, posing a serious threat to the ecological environment and human health [4-5]. Tetracycline (TC), as a representative of tetracycline antibiotics, has drawn significant attention for its residual presence in wastewater. Developing green and sustainable technologies to efficiently treat such antibiotics has become a critical task.

Among the treatment methods for TC-containing wastewater, traditional technologies such as coagulation-sedimentation, flotation, and activated sludge processes, although well-developed and widely applied, generally suffer from low treatment efficiency [6]. Emerging processes like advanced oxidation and membrane treatment are capable of completely removing pollutants, but their complex operating conditions and high equipment costs make large-scale promotion and application difficult. Adsorption-based methods present considerable operational advantages, marked by exceptional removal efficiency. requiring modest capital expenditure and straightforward operational protocols. thereby demonstrating significant promise for real-world implementation. Although the treatment effectiveness of this method may be constrained by factors such as adsorbent selectivity and process operating conditions, leading to potential issues of pollutant residue, because it typically serves as a pretreatment step in integrated treatment processes, such residue problems can be effectively resolved by

subsequent treatment units.

Chitosan (CS) is a biomass material derived from the deacetylation of chitin from crustaceans like shrimp and crab. It originates from abundant, low-cost raw materials and is widely employed in various fields such as biomedical engineering and wastewater treatment. Due to the abundance of active groups (−OH, $-NH_2$, and C−O−C) in its molecular structure, CS can capture pollutants through complexation, hydrogen bonding, etc., making it highly favored in the field of adsorption [9]. However, the low solubility of CS in neutral or high pH solvents greatly limits its application. Improving the water solubility of chitosan through carboxymethylation is a currently viable solution. This process is achieved by mixing chitosan and chloroacetic acid in an alkaline medium [10-11]. Carboxymethyl chitosan (CMCS) not only has good solubility over a wide pH range but also retains the non-toxicity and biocompatibility of natural chitosan, making it a superior adsorbent material [12-13].

The separation of the adsorbent from the liquid phase represents a pivotal step in the overall adsorption process. Efficient separation is a prerequisite for ensuring the treated solution meets standards and avoids secondary pollution, and is crucial for improving the economic and environmental friendliness of the process. Aerogels are easy to separate and have strong stability. Therefore, using adsorbents in the form of aerogels for adsorption is a rational and efficient choice. Fe^{3+}, due to its high charge density and hard acid characteristics, easily forms coordination bonds with negatively charged O and N atoms in −OH, −COOH, and $-NH_2$ groups: the O and N atoms in these groups are rich in lone pair electrons and can act as electron donors, combining with the empty orbitals of Fe^{3+} (electron acceptor) to form stable coordination structures [14-17]. Introducing trivalent metal ions like Fe^{3+} into CMCS can initiate the gelation process through the coordination between Fe^{3+} and CMCS [18-19]. Based on this, this study dripped CMCS solution into an Fe^{3+} solution, utilizing Fe^{3+} to initiate gelation to obtain hydrogel beads, which were then freeze-dried to obtain a morphologically stable composite aerogel material.

This study innovatively proposes a simple and low-cost method, successfully preparing a novel Fe^{3+}-functionalized CMCS composite aerogel (CMCS@Fe^{3+}) and applying it for TC adsorption. A comprehensive array of analytical methodologies was employed to examine the structural attributes of the composite and elucidate the underlying principles governing its sorption behavior.

2 Experimental Design

2.1 Materials

Carboxymethyl chitosan (CMCS, deacetylation degree exceeding 90%, substitution degree 90%) was procured from Shanghai Macklin Biochemical Technology Co., Ltd. HCl, NaOH and $FeCl_3·6H_2O$ were supplied by Beijing Innochem Science & Technology Co., Ltd. NaCl, KCl, $CaCl_2$ were obtained from Shanghai Aladdin Biochemical Technology Co., Ltd. TC, 96% purity and $MgCl_2$, 99% purity)were sourced from Shanghai McLean Biochemical Co., Ltd.

2.2 Synthesis of CMCS@Fe^{3+} Aerogel

The synthetic protocol for the composite adsorbent is illustrated schematically in Figure 1. Initially, 4.0 grams of carboxymethyl chitosan powder was dispersed into 100 milliliters of ultrapure water and subjected to continuous agitation for a duration of 12 hours to achieve a homogeneous solution. Simultaneously, 2 g of $FeCl_3·6H_2O$ was dissolved in 200 mL of deionized water to prepare another solution. Then, the CMCS solution was uniformly dripped into the $FeCl_3$ solution using a syringe. Following a 24-hour solidification period, the hydrogel beads were retrieved and washed repeatedly with deionized water until the eluate reached neutral pH. Subsequently, the purified hydrogel beads were subjected to lyophilization at -50°C under vacuum for 36 hours to yield the CMCS@Fe^{3+} aerogel.

In addition, this study also designed material comparison experiments: Given that the coordination ability of Fe^{3+} is much higher than that of Ca^{2+}, Ca^{2+} was used as a substitute ion, and a series of comparative samples were prepared by controlling their molar ratio. Specifically, $FeCl_3·6H_2O$ (1.5, 1.0, 0.5, 0 g) and corresponding masses of $CaCl_2$ (0.24, 0.47, 0.71, 0.94 g) were weighed for each group. Each mixture was co-dissolved in 200 mL of ultrapure water to construct aerogel systems with Fe^{3+} to Ca^{2+} molar ratios of 3:1, 1:1, 1:3, and 0:1, in order to

investigate their adsorption performance.

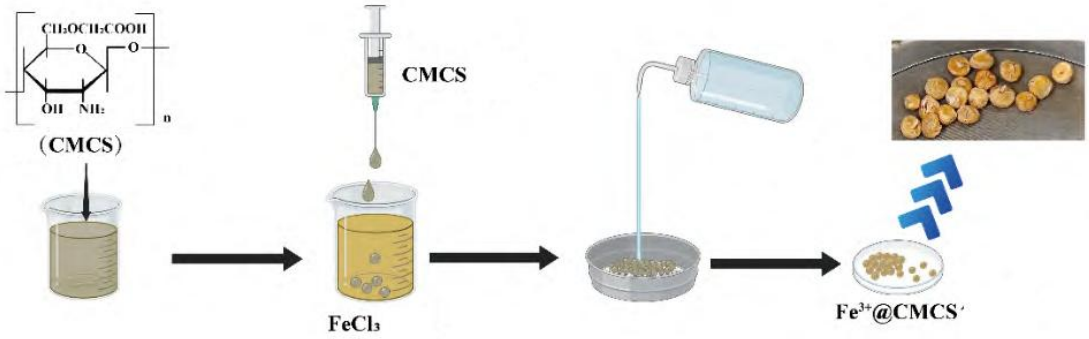

Figure 1 Schematic diagram of CMCS@Fe^{3+} aerogel preparation

2.3 Adsorption Experiments

An accurately measured 20-milligram aliquot of CMCS@Fe^{3+} composite was transferred into a 100-milliliter conical flask, followed by the addition of 30 milliliters of tetracycline solution at a concentration of 50 milligrams per liter. The initial hydrogen ion concentration was modulated to values ranging from 3.0 to 9.0 utilizing 0.1 molar hydrochloric acid or sodium hydroxide solutions. The reaction mixture was subsequently subjected to oscillatory incubation in a thermostated water bath at 298 Kelvin and 180 revolutions per minute, maintained under dark conditions for 24 hours, to systematically evaluate the influence of initial pH on sorption performance. Following this, the impact of varying adsorbent loadings ranging from 15 to 35 milligrams was systematically investigated. Additionally, employing the previously determined optimal pH conditions and adsorbent loading, the temporal sorption dynamics were examined for tetracycline solutions at initial concentrations of 25 and 50 milligrams per liter, respectively. Additionally, isothermal adsorption measurements were performed at 298, 308, and 318 K to establish complete equilibrium isotherms. Upon completion of the sorption process, the resultant mixture was subjected to centrifugal separation, and the obtained supernatant was subsequently passed through membrane filters of 0.45 micrometer and 0.22 micrometer pore sizes in sequential order. The tetracycline concentration was quantified utilizing HPLC. The separation was conducted at a column temperature of 30 degrees Celsius, with ultraviolet detection performed at a wavelength of 365 nanometers. The mobile phase consisted of a binary mixture comprising 0.01 molar oxalic acid solution and acetonitrile in a volumetric ratio of 70:30, delivered at a constant flow rate of 1 milliliter per minute. The elimination efficiency and sorption capacity of tetracycline were computed employing Equations (1) and (2), respectively.

$$qt=(C0-Ct)V/m \quad ((1)$$

$$R\%=(C0-Ct)/C0\times100\% \quad (2)$$

Where:

Qt – Adsorption capacity at time t, mg/g; C0 – Initial mass concentration of TC, mg/L; Ct – Residual mass concentration of TC at time t, mg/L; V– Solution volume, L; m– Dosage of CMCS@Fe^{3+}, g; R– Removal rate of TC, %.

2.4 DFT Calculations

To illuminate the underlying sorption mechanisms governing tetracycline uptake by CMCS@Fe^{3+}, the binding energetics were assessed via computational simulations employing Density Functional Theory. A fully deacetylated O-carboxymethyl chitosan disaccharide unit (containing one $–CH_2COOH$ and one $–NH_2$) was used to simulate the CMCS matrix. Fe^{3+} (high-spin d^5) has hard acid character and mainly forms hexacoordinate

octahedral structures with O-donor ligands (such as water, carboxylate) [20-21]. Considering that Fe^{3+} will first coordinate and crosslink with CMCS, a representative model where Fe^{3+} chelates with carboxyl groups in a bidentate manner to form a stable structure can be adopted [22]. Furthermore, to optimize calculation time, acetic acid molecules (CH_3COOH) can be used to simulate the carboxymethyl structure in CMCS. Based on this, this study constructed the Fe^{3+} coordination environment as $[Fe(OOCCH_3)_2(bidentate)(H_2O)_2]^+$ (double carboxylate bidentate chelation occupying equatorial positions, axial H_2O as adsorption sites), with a charge number set to +1. For the optimal initial adsorption pH environment (pH=7.0), tetracycline exists as neutral TC^0, with a charge number set to 0. Calculations were performed using the Material Studio 2019 program. All computational models underwent geometric optimization via the Becke-Lee-Yang-Parr (BLYP) exchange-correlation functional implemented in the $Dmol^3$ software package. incorporating DFT-D dispersion corrections via the Grimme approach, with aqueous solvation effects accounted for in the simulation environment. AutoDock Vina [23] was used to search for the optimal binding configuration between TC and the CMCS dimer, with all parameters set to default for automated molecular docking. For the coordination binding between Fe^{3+} and TC, manual molecular docking was performed based on the electrostatic potential on the surface functional groups of the TC molecule. Subsequently, the obtained structures were imported into the $Dmol^3$ module for further optimization. Finally, the average adsorption free energy (E ads) between the adsorbent and adsorbate was calculated to evaluate the adsorption strength of different modules in CMCS@Fe^{3+} for TC.

2.5 Feasibility of Adsorbent Application in Composite Wastewater

To verify the feasibility of CMCS@Fe^{3+} application in composite wastewater, a systematic assessment was conducted through adsorption-desorption cycling experiments, background ionic strength effect experiments, and simulated wastewater adsorption experiments.

The stability of the adsorbent in practical application was evaluated through adsorption-desorption cycling experiments. An aliquot of 20 milligrams of CMCS@Fe^{3+} composite was introduced into 30 milliliters of tetracycline solution at a concentration of 10 milligrams per liter. Following pH adjustment to 7.0, the sorption process was conducted in a thermostated shaking water bath at 298 Kelvin and 180 revolutions per minute. After adsorption, the aerogel was transferred to a conical flask containing 40 mL of methanol and oscillated at 298 K, 180 r/min for 12 h for regeneration. After rinsing 5 times with ultrapure water, it was 投入 a new cycle. A total of 8 cycles were performed.

The presence of typical inorganic cations in real wastewater—including sodium, potassium, magnesium, and calcium ions—can suppress tetracycline uptake via competitive binding and electrostatic perturbation effects. To this end, adsorption trials were performed employing 30 mL of tetracycline solution (initial concentration: 10 mg/L) to evaluate how varying ionic strengths (0–10 g/L) of the aforementioned cations, serving as background electrolytes, influenced the TC removal efficiency of CMCS@Fe^{3+}.

Furthermore, the sorption efficacy of the adsorbent was evaluated in ultrapure water, municipal tap water, surface freshwater, and synthetic wastewater matrices. The simulated wastewater was prepared with reference to the "Guangdong Province Livestock and Poultry Breeding Industry Pollutant Discharge Standard" (DB 44/613-2024): Dissolve 400 mg glucose, 75 mg urea, and 28 mg K_2HPO_4 in 1 L of ultrapure water to obtain synthetic wastewater. Lake water was taken from the central lake of Guangzhou University City. For the experiment, using water of different qualities as the solvent, prepare 30 mL solutions containing 1000 μg/L, 500 μg/L, and 100 μg/L TC, respectively. Add 20 mg of CMCS@Fe^{3+} to each for adsorption experiments.

3 Results and Discussion

3.1 Characterization

The scanning electron micrographs presented in Figure 2 illustrate the surface morphology and cross-sectional architecture of the CMCS@Fe^{3+} composite material. The material surface is covered with wrinkles and distributed with several deep cracks, and the spherical contour has deviated from a regular shape. Enlargement of the crack area reveals: A three-dimensional interconnected porous network structure is constructed inside

the cracks, formed by interwoven slender fibrous basic units forming a continuous network skeleton. From the cross-sectional image, it is observed that the material interior is composed of radially arranged layered units, with the structure extending in a "divergent" manner from the center to the edge. Enlargement of the internal area shows that the interlayer pores are looser than the surface crack area, forming a more open porous system. The surface cracks and internal porous structure collaboration promote the mass transfer of TC to the surface and interior of the adsorbent.

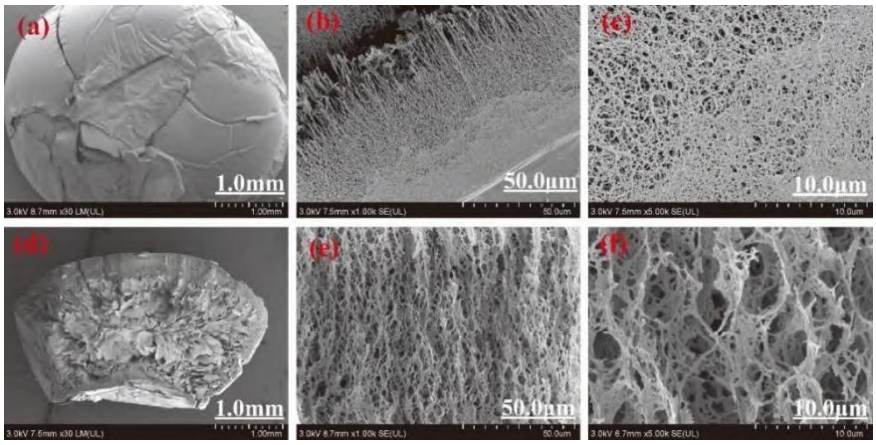

Figure 2 SEM images of CMCS@Fe^{3+} surface (a-c) and cross section (d-f)

The nitrogen adsorption-desorption isotherms for pristine CMCS and the CMCS@Fe^{3+} composite are depicted in Figure 3.In the low relative pressure region, the N_2 adsorption amount of CMCS@Fe^{3+} increases sharply. When $P/P_o > 0.6$, the desorption curve exhibits typical Type IV isotherm characteristics accompanied by a hysteresis loop, which is an important logo of materials having microporous and mesoporous structures [24]. Their specific surface areas are 26.75 m^2/g and 8.30 m^2/g, respectively. This result indicates: Fe^{3+}, by virtue of its strong coordination ability, can simultaneously bind with oxygen-containing functional groups and amino groups in CMCS, forming a multiple cross-linked network. This structural configuration effectively prevents the compact aggregation of polymer chains, thereby substantially enhancing the porous architecture of the material. concomitantly augmenting its specific surface area to a moderate extent, and creating advantageous conditions for tetracycline uptake via pore-filling mechanisms.

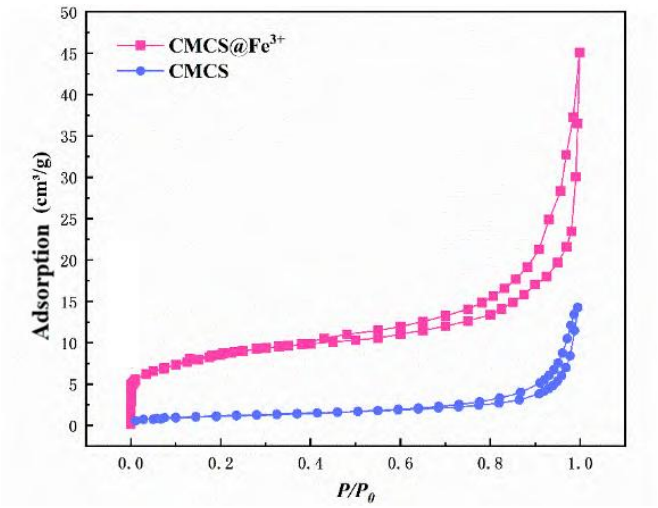

Figure 3 N_2 adsorption-desorption isotherm

3.2 Batch Adsorption Experiments

3.2.1 Effect of Initial Solution pH and Adsorbent Dosage on Adsorption

The electrokinetic potential measurements for CMCS@Fe^{3+} across a range of pH conditions are presented in Figure 4(a), revealing an isoelectric point near pH 7.5. Tetracycline, being an amphoteric compound with pKa values of 3.3, 7.7, and 9.7, exhibits speciation-dependent behavior in aqueous media across varying pH regimes: At pH below 3.3, the cationic form TC^+ prevails; pH 3.3 -7.7, the zwitterionic species TC^o is dominant; while in the pH range of 7.7 to 9.7, the anionic form TC^- becomes predominant [25]. The influence of initial pH on adsorption capacity is illustrated in Figure 4(b). At pH 3.0, pronounced electrostatic repulsion arises between the positively charged TC^+ species and the similarly charged CMCS@Fe^{3+} surface, thereby impeding adsorption. Sorption efficacy exhibits a progressive enhancement within the pH interval of 4.0–7.0, demonstrating elevated removal performance across the pH range of 5.0–8.0. The sorption capacity attains its peak value of 66.46 milligrams per gram, accompanied by a removal efficiency of 88.62%, under neutral conditions at pH 7.0. Within this pH regime, tetracycline predominantly exists in its zwitterionic form (TC^o). suggesting that electrostatic attraction contributes minimally to the overall sorption mechanism. At pH values exceeding 8.0, the zwitterionic species progressively transforms into the anionic form (TC^-), thereby inducing a secondary reduction in sorption efficacy attributable to electrostatic repulsive forces. All subsequent experimental investigations were therefore conducted under neutral conditions at pH 7.0.

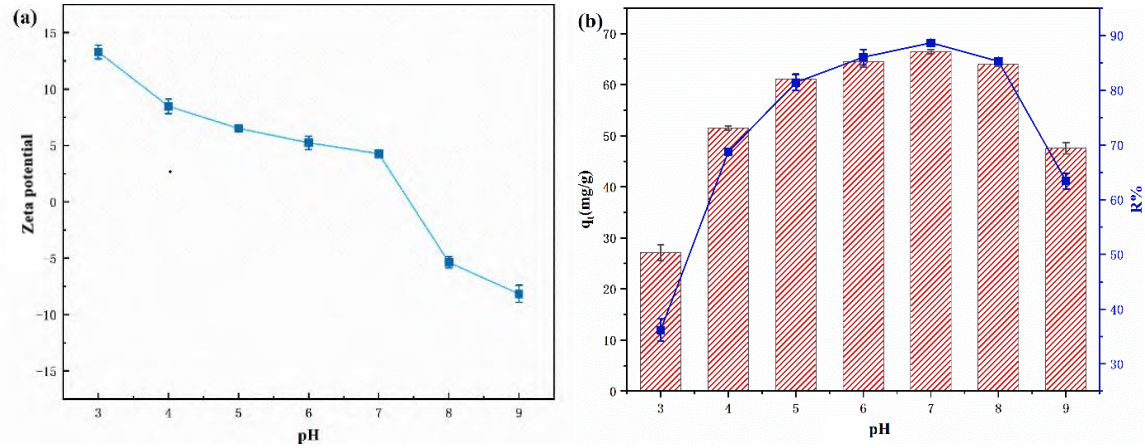

Figure 4 (a) ζ potential of CMCS@Fe^{3+} at different pHs; (b) Effect of pH on the adsorption efficiency

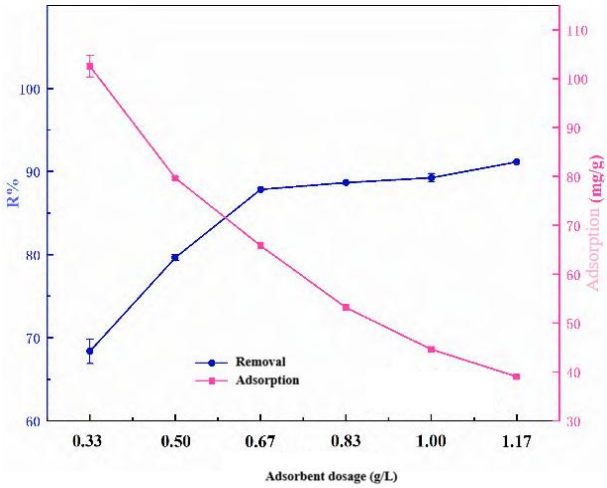

Figure 5 Effect of CMCS@Fe^{3+} dosage on adsorption performance

To investigate the effect of CMCS@Fe^{3+} dosage on TC adsorption performance, related experimental studies were conducted. The experimental results shown in Figure 5 indicate: With increasing adsorbent loading,the tetracycline elimination efficiency exhibits substantial enhancement. Upon surpassing an adsorbent concentration of 0.67 grams per liter, the enhancement in removal efficiency decelerates, while the specific sorption capacity exhibits a pronounced decline. To facilitate the adsorbent in achieving maximal overall

performance, a loading concentration of 0.67 grams per liter was employed for all subsequent investigations.

3.2.2 Kinetics

Figure 6(a) shows the change of TC removal efficiency by CMCS@Fe^{3+} over time. The results show that in the initial stage of adsorption (0–2 h), due to the abundance of active sites on the adsorbent surface, the large concentration gradient of adsorbate, and small mass transfer resistance, the adsorption rate is extremely fast. Equilibrium was attained within approximately 24 hours for an initial tetracycline concentration of 25 mg/L, whereas 60 hours were required to reach saturation at 50 mg/L. To thoroughly investigate the kinetic behavior of the adsorption process, the pseudo-first-order and pseudo-second-order kinetic models (Equations 3 and 4) were employed for data fitting, with the corresponding parameters summarized in Table 1. The pseudo-second-order model exhibited superior correlation coefficients (R^2 = 0.998 and 0.993), suggesting that chemisorption governs the rate-limiting step of the adsorption process.

$$qt=qe(1-e^{-k1t}) \quad (3)$$

$$qt=k_2q_e^2t/(1+k_2q_et) \quad (4)$$

Where:

qe– Adsorption capacity at equilibrium, mg/g; k1 and k2– Pseudo-first-order and pseudo-second-order kinetic rate constants, g/(mg·h) and g/(mg·h), respectively; t– Contact time, h.

Table 1 Parameters for Pseudo-first order and Pseudo second-order kinetic fitting

C0 (mg/L)	qe,exp (mg/g)	k1 (h^{-1})	Pseudo-first order qe,cal (mg/g)	R2	k2 (g/(mg·h))	Pseudo-second order qe,cal(mg/g)	R2
25	34.83	0.216	35.03	0.985	0.0057	41.60	0.993
50	72.96	0.178	69.27	0.988	0.0028	78.90	0.998

CMCS@Fe^{3+} has a porous internal system. To reveal whether intraparticle diffusion is the rate-controlling step for adsorption, the intraparticle diffusion model (Equation (5)) was used to simulate the adsorption kinetics. The regression outcomes are presented in Table 2 and illustrated in Figure 6(b), with the isotherm profiles segmented into three distinct regions: The initial phase encompasses rapid external mass transfer of tetracycline molecules to the adsorbent surface, accompanied by a steep rise in uptake capacity. The subsequent phase involves the slow migration of TC molecules from the exterior into the internal porous network, resulting in a decelerated adsorption rate. The final phase exhibits a plateau in the uptake curve, indicating the system approaching saturation equilibrium. Additionally, the non-zero intercepts observed for all kinetic profiles confirm that intraparticle diffusion alone does not govern the overall adsorption rate.

$$qt=k_dt^{1/2}+L \quad (5)$$

Where:

kd– Intraparticle diffusion rate constant, mg/(g·$h^{1/2}$); L– Boundary layer thickness, mg/g.

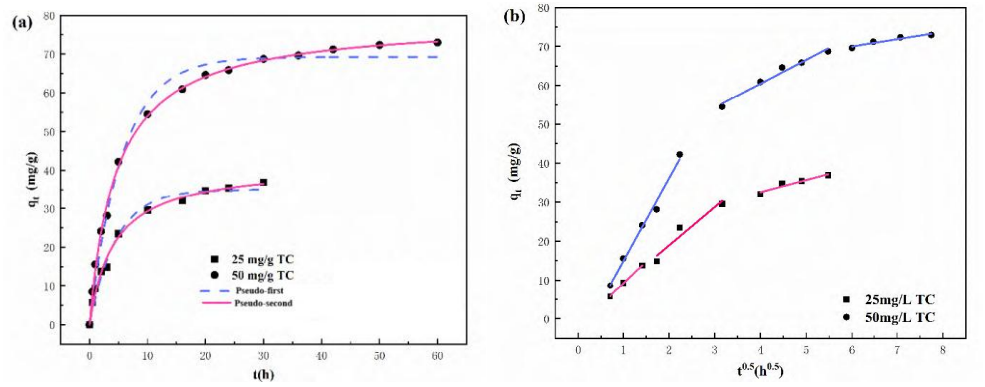

Figure 6 (a) Pseudo first-order and Pseudo second-order kinetic model fitting; (b) intraparticle diffusion model plots fitting

Table 2 Parameters of the intraparticle diffusion model

C0(mg/L)	Stage 1		Stage 2		Stage 3	
	ki,1($mg\cdot g^{-1}\cdot h^{-0.5}$)	R_1^2	ki,2($mg\cdot g^{-1}\cdot h^{-0.5}$)	R_2^2	ki,3($mg\cdot g^{-1}\cdot h^{-0.5}$)	R_3^2
25	11.29	0.998	9.849	0.964	3.150	0.945
50	21.22	0.990	6.157	0.975	1.857	0.967

3.2.3 Adsorption Isotherms and Adsorption Thermodynamic Analysis

Figure 7 presents the adsorption isotherms of TC on CMCS@Fe^{3+} at different temperatures. The equilibrium adsorption capacity for TC increased with rising temperature and showed nonlinear growth with increasing equilibrium concentration, indicating the adsorption process is dominated by chemisorption, rather than surface physical adsorption.

The equilibrium data were modeled using Langmuir, Freundlich, and Sips [26] isotherm equations (Equations 6–8), with the regression parameters presented in Table 3. The Sips model exhibited the strongest correlation (R^2 = 0.991, 0.992, and 0.990), markedly surpassing the predictive capability of the alternative models. This suggests that the adsorption mechanism is governed by both a finite monolayer coverage limit and the non-uniform energetic landscape of the adsorbent surface [27]. Remarkably, the Sips model predicted an exceptionally high maximum uptake capacity of 785.85 mg/g at 298 K. This value surpasses most adsorbents listed in Table 4, demonstrating that CMCS@Fe^{3+} is undoubtedly a highly promising adsorbent.

$$qe=q_mK_LC_e/(1+K_LC_e) \quad (6)$$

$$qe=K_FCe^{1/nF} \quad (7)$$

$$qe=qm(K_sC_e)^{ns}/[1+(K_sCe)^{ns}] \quad (8)$$

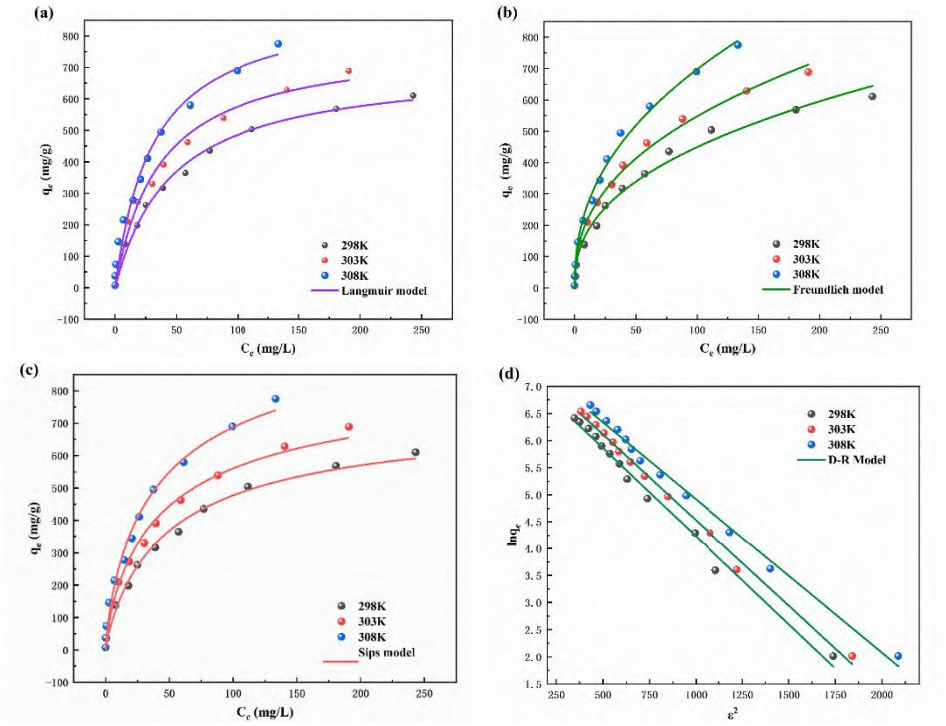

Figure 7 Adsorption isotherms: (a) Langmuir; (b) Freundlich; (c) Sips; (d) D-R linear adsorption isotherm

To facilitate a more profound elucidation of the underlying sorption mechanisms, the Dubinin-Radushkevich isotherm model was incorporated into the analytical framework. This theoretical framework enables discrimination between physisorption and chemisorption mechanisms through quantification of the mean adsorption free energy (E_ads). thereby disclosing the fundamental nature of the sorption process. As determined through the Dubinin-Radushkevich linearized model (Equations 9–11), the calculated mean free energy values at various temperatures consistently exceed 8 kilojoules per mole, thereby signifying that chemisorption constitutes the predominant mechanism governing tetracycline uptake onto CMCS@Fe^{3+}. [29-30]

$$\ln q_e = \ln q_m - B\varepsilon^2 \quad (9)$$

$$\varepsilon = RT \ln(1+1/C_e) \quad (10)$$

$$E_{ads} = 1/\sqrt{2B} \quad (11)$$

Where:

Ce– Equilibrium concentration of TC, mol/L; B– Constant related to adsorption energy, mol^2/kJ^2; ε– Polanyi potential, kJ/mol; R– Gas constant, 8.314 J/(mol·K); T– Absolute temperature, K.

Table 3 Adsorption isotherm parameters

Model	Parameter	T=298 K	T=303 K	T=308 K
Langmuir	qm($mg \cdot g^{-1}$)	710.00	783.97	914.35
	KL($L \cdot mg^{-1}$)	0.0217	0.0276	0.0321
	R2	0.987	0.980	0.979
Freundlich	KF($mg \cdot g^{-1}$)	69.29	83.84	97.26
	nF	2.4637	2.4546	2.3375

Model	Parameter	T=298 K	T=303 K	T=308 K
	R2	0.989	0.986	0.990
Sips	qm($mg·g^{-1}$)	785.85	879.78	1060.54
	Ks($L·mol^{-1}$)	$8.59×10^3$	$9.10×10^3$	$9.72×10^3$
	ns	0.8670	0.6872	0.7798
	R2	0.991	0.992	0.990
D-R	qm($mg·g^{-1}$)	772.78	1242.65	1459.72
	B($mol^2·kJ^{-2}$)	0.00327	0.00302	0.00284
	Eads($kJ·mol^{-1}$)	12.36	12.86	13.27
	R2	0.987	0.994	0.989

Table 4 Comparison of adsorption efficiency of TC by different adsorbents

Adsorbent	Dosage ($g·L^{-1}$)	T (K)	qm($mg·g^{-1}$)	Ref.
Walnut shell-based alkali-activated biochar (KWS900)	/	318	607.00 ± 31.87	[31]
ZIF-8-chitosan composite microspheres	0.5	293	495.04	[32]
Magnetic chitosan (CS-Fe_3O_4)	0.5	293	211.21	[33]
Ethanolamine-functionalized magnetic graphene (MAEGO)	0.2	303	315.25	[34]
Amino-functionalized Fe_3O_4@SiO_2 crosslinked sodium alginate (Fe_3O_4@SiO_2-NH_2/SA)	0.1	310	588.41	[35]
Aluminosilicate zeolite nanoparticles	/	298	454.55	[36]
Alginate-halloysite loaded molecularly imprinted polymer beads (ALG_Hal@MIP)	0.2	298	281.0	[37]
Montmorillonite/sodium alginate composite beads	5.0	298	745.0	[38]
Three-dimensional porous carbon nanofiber/graphene oxide composite aerogel (PCNF/GOAs)	0.2	298	947.1	[39]
Fe^{3+} functionalized carboxymethyl chitosan aerogel (CMCS@Fe^{3+})	**0.67**	**298**	**785.85**	**This work**

Table 5 Thermodynamic parameters of CMCS@Fe^{3+} adsorption of TC

T (K)	lnK0	ΔG∘($kJ·mol^{-1}$)	ΔH∘($kJ·mol^{-1}$)	ΔS∘($J·mol^{-1}·K^{-1}$)
298	9.058	-22.443		
303	9.116	-22.964	9.426	106.926
308	9.182	-23.513		

3.3 TC Adsorption Mechanism

3.3.1 FT-IR and XPS

As shown in the FT-IR spectral analysis in Figure 8: Before adsorption, the C–H bond stretching vibrations of CMCS@Fe^{3+} correspond to two absorption peaks at 1325.95 cm^{-1} and 2929.73 cm^{-1}; The band at 1629.12 cm^{-1} corresponds to the superimposed signals arising from the asymmetric stretching of carboxylic acid groups and the N–H bending vibration. The absorption band at 1407.82 cm^{-1} is assigned to the symmetric stretching mode of carboxylate anions, whereas the peak observed at 1073.02 cm^{-1} originates from ether linkage (C–O–C) stretching vibrations. The broad feature centered at 3424.40 cm^{-1} results from the convolution of O–H and N–H stretching vibrational modes. After adsorption, the O–H and N–H stretching vibration peak shifts to 3431.71 cm^{-1}, and the characteristic absorption peaks of $–COO^-$ and C–O–C also show slight shift. On this basis, it is postulated that oxygen-bearing functionalities (hydroxyl, carboxyl, and ether groups) along with amino moieties present in CMCS@Fe^{3+} can engage in hydrogen bonding interactions with tetracycline molecules.

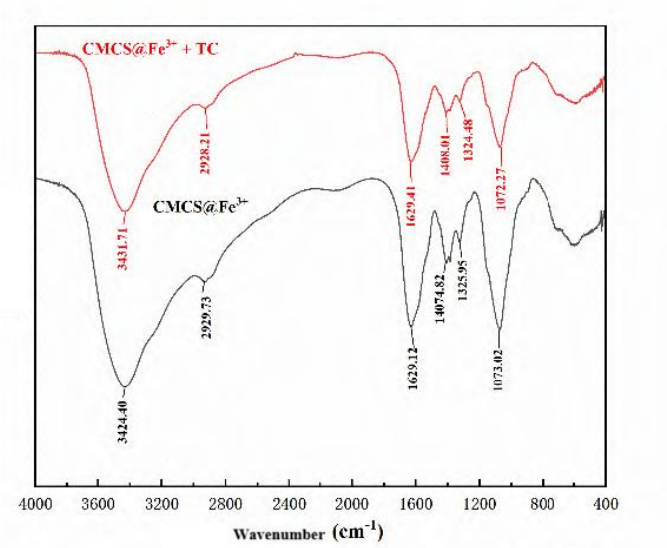

Figure 8 FT-IR spectra of CMCS@Fe^{3+} before and after adsorption of TC

The X-ray photoelectron spectroscopic data for CMCS@Fe^{3+} prior to and following tetracycline uptake are presented in Figures 9(a) through 9(e). The survey spectrum and high-resolution C 1s region reveal a pronounced enhancement in the characteristic C–C bond signal intensity subsequent to tetracycline uptake. attributable to the cumulative contribution of abundant C–C bonds originating from the successfully immobilized tetracycline molecules superimposed upon the existing spectral signal. In the O 1s spectrum, the fresh adsorbent shows three fitted peaks at 532.8 eV (C–O–C), 531.31 eV (–OH), and 529.84 eV (C=O). Following tetracycline uptake, all spectral components exhibit a shift toward elevated binding energies, accompanied by a marked diminution in the relative intensity of the C–O–C characteristic peak. Within the N 1s spectral region, both the amino ($–NH_2$) and carbon-nitrogen (C–N) components demonstrate a shift toward higher binding energies post-adsorption, concomitant with a reduction in their respective integrated peak areas. This observation substantiates that hydrogen bonding interactions between CMCS@Fe^{3+} and tetracycline constitute a significant contributor to the overall sorption mechanism. the pristine adsorbent exhibits characteristic signals at binding energies of 710.79 electron volts and 724.19 electron volts, which correspond to the spin-orbit coupled doublet arising from the Fe $2p_3/_2$ and Fe $2p_1/_2$ electronic states, respectively, Characteristic spectral signatures corresponding to iron in both divalent (Fe^{2+}) and trivalent (Fe^{3+}) oxidation states are observed in the data [42]. After TC loading, the area of all characteristic peaks for Fe^{3+} decreases significantly, indicating that Fe^{3+} in the material forms coordination interactions with oxygen-containing groups and amino groups in TC via unsaturated metal centers, thereby promoting efficient capture of TC.

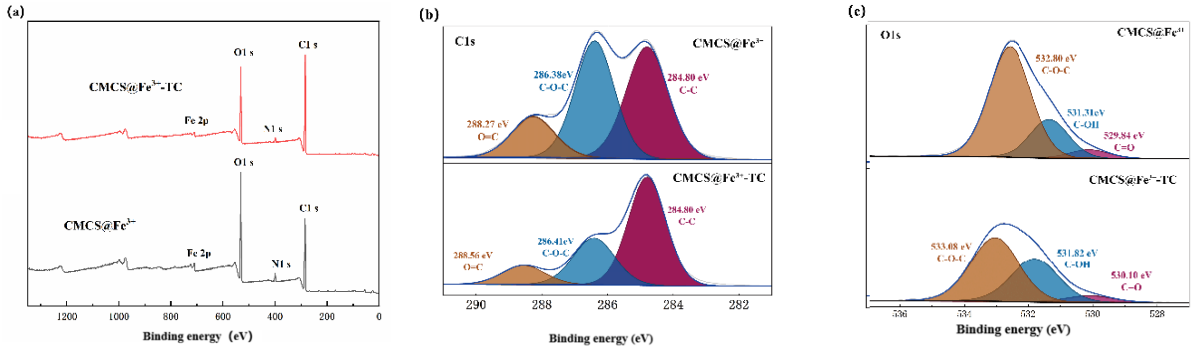

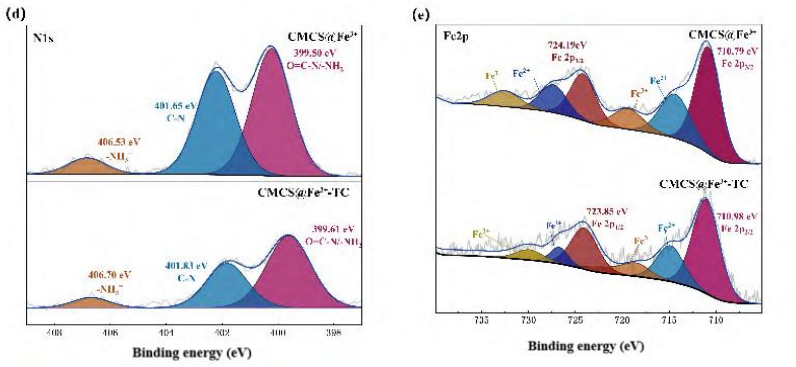

Figure 9 (a) Full-band XPS scans of CMCS@Fe^{3+} before and after adsorption; high-resolution spectra of (b) C 1s, (c) O 1s, (d) N 1s, and (e) Fe 2p of CMCS@Fe^{3+} before and after adsorption

3.3.2 DFT Calculations

Molecular-level insights into tetracycline (TC) adsorption behavior were gained via computational modeling based on Density Functional Theory (DFT). From Figure 10(a), it can be seen that the areas around O and N atoms in the TC molecule carry obvious negative charge, enabling them to act as electron donors and becomes potential binding sites for coordination with Fe^{3+}. Figures 10(b)-(d) present possible binding structures between the TC molecule and $(Fe(OOCCH_3)_2(H_2O)_2)^+$ as well as CMCS. The model where CMCS and TC are connected via multiple hydrogen bonds has an EAds of -37.38 kcal/mol, whereas the Eads for Fe^{3+} coordinating with the $–NH_2$ and –OH functional groups in the TC molecule are -39.21 kcal/mol and -33.32 kcal/mol, respectively. These data indicate that both hydrogen bonding and Fe^{3+} coordination are important mechanisms for TC capture by CMCS@Fe^{3+}. It is worth noting that in the actual material, CMCS may only occupy some Fe^{3+} sites, and Fe^{3+} can form multidentate coordination with TC. The Eads calculated for this mode may be much lower than that in this study's model, highlighting the core role of Fe^{3+} coordination in the adsorption mechanism.

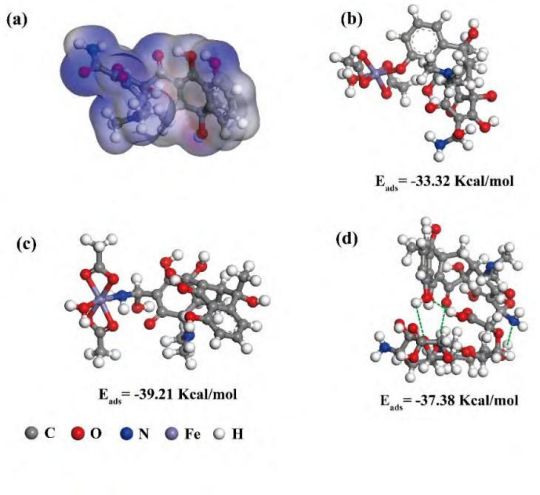

Figure 10(a) Electrostatic potential analysis of TC; average adsorption free energy of (b) CMCS binding to TC via hydrogen bonding, and $(Fe(OOCCH_3)_2(H_2O)_2)^+$ binding to TC via coordination (c) and (d).

3.3.3 Material Comparison Experiments

Figure 11 presents the adsorption performance of composite materials with different Fe^{3+}:Ca^{2+} molar ratios for TC: Elevated proportions of this component correlate with enhanced tetracycline (TC) uptake performance by the composite material. When the material contains no Fe^{3+}, its average adsorption capacity for TC is only 12 mg/g. At this time, TC is adsorbed mainly through hydrogen bonding and weak coordination by Ca^{2+}. This phenomenon is attributed to: During the material gelation stage, CMCS has already consumed a large number of coordination sites of Ca^{2+}. The remaining sites, after binding with TC, are prone to drop, resulting in weak TC

capture. These experimental results further confirm that Fe^{3+}, by virtue of its unsaturated center coordination, is the core mechanism for the material's efficient TC removal.

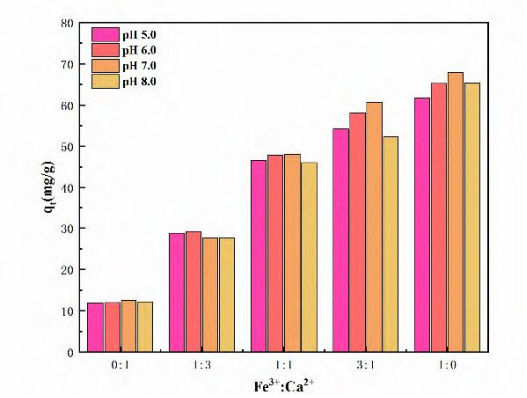

Figure 11 Effect of different Fe^{3+}:Ca^{2+} molar mass ratios on TC adsorption efficiency

In summary, hydrogen bonding and Fe^{3+} coordination are two important mechanisms for TC adsorption by CMCS@Fe^{3+}. The fundamental mechanism involves the establishment of coordination bonds between ferric cations (Fe^{3+}) and the negatively charged functional moieties embedded within the tetracycline molecular framework. This mechanism functions cooperatively with hydrogen bonding interactions formed between the oxygen- and nitrogen-containing functional groups of carboxymethyl chitosan and the tetracycline molecules. Furthermore, pore-filling effects contribute to the adsorption process, as substantiated by the aforementioned physicochemical characterization findings. Additionally, the involvement of cation-π interactions between ferric ions (Fe^{3+}) and the aromatic moieties of tetracycline (TC) cannot be ruled out. This phenomenon stems from electrostatic forces coupled with partial electron delocalization occurring between positively charged ferric ions (Fe^{3+}), acting as electron-deficient centers, and the extended π-conjugated electron cloud of the aromatic ring system serving as the electron-rich donor. This stabilization arises from the establishment of robust cation-π complexes, as documented in prior literature [43-44]. A schematic representation delineating the underlying adsorption mechanism for tetracycline (TC) is presented in Figure 12.

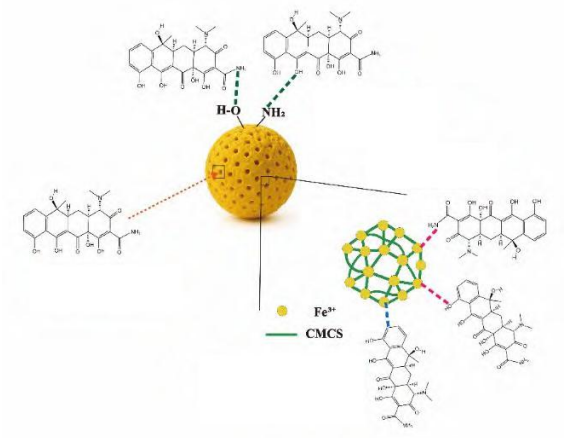

Figure 12 Schematic diagram of the adsorption mechanism of TC

3.4 Feasibility Assessment of Adsorbent Application in Composite Wastewater

The influence of repeated adsorption-desorption cycles on tetracycline (TC) removal efficiency is depicted in Figure 13(a). As the number of cycles increases, the TC removal rate gradually declines. This is mainly attributed to: Loss of adsorbent during the TC desorption process using methanol, and potentially incomplete desorption. Nonetheless, after 8 cycles, the TC removal rate for CMCS@Fe^{3+} can still reach 85.20%, indicating it is an excellent

adsorbent material combining stability and economic efficiency.

The presence of ubiquitous inorganic cations—including sodium (Na^{+}), potassium (K^{+}), calcium (Ca^{2+}), and magnesium (Mg^{2+})—commonly encountered in authentic composite wastewater matrices, may exert inhibitory or disruptive effects on tetracycline (TC) adsorption. To examine this phenomenon, the impact of varying ionic strength conditions on tetracycline (TC) uptake by the CMCS@Fe^{3+} composite was systematically evaluated. The obtained experimental outcomes are visually summarized in Figure 13(b): Across the investigated ionic concentration span of 0 to 10 g/L, the decline in tetracycline (TC) removal efficiency remains comparatively modest. This phenomenon stems from the fact that the TC adsorption process relies much less on electrostatic attraction compared to other mechanisms such as hydrogen bonding and Fe^{3+} coordination. Thus, this material exhibits excellent environmental adaptability.

Figure 13(c) compares TC removal rates under different water qualities: For an initial TC concentration of 1000 μg/L, the TC removal rates in all four water qualities exceed 90%; in the simulated aquaculture wastewater system, the removal rate for 100 μg/L TC decreases to 73.72%, but it is still at a relatively high level. It is evident that CMCS@Fe^{3+} generally performs well in removing trace TC under different water qualities, further confirming its application potential in composite wastewater treatment.

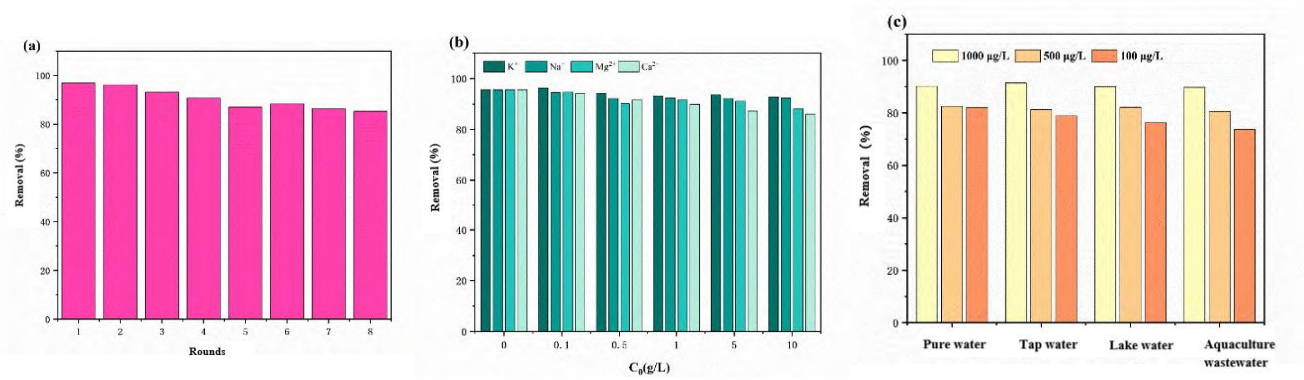

Figure 13(a) CMCS@Fe^{3+} adsorption-desorption cycle; (b) effect of inorganic salt ions on TC removal; (c) comparison of TC removal rates under different water qualities

4 Conclusion

This study successfully prepared a uniform, stable, and easily separable CMCS@Fe^{3+} aerogel adsorbent by utilizing the coordination between Fe^{3+} and CMCS for cross-linking. The coordination of Fe^{3+} not only enhanced the stability of the adsorbent but also participated as a key adsorption site in the efficient adsorption of TC.

The as-prepared adsorbent exhibits a hierarchical porous architecture comprising both microporous and mesoporous domains, with the incorporation of ferric ions (Fe^{3+}) further augmenting its specific surface area. The fabricated composite material demonstrates superior adsorption performance under weakly acidic to neutral conditions (pH 5.0–8.0). The Sips isotherm model yields a predicted maximum uptake capacity of 785.85 mg/g at 298 K, which represents a substantially elevated value. Synergistic effects exist between CMCS and Fe^{3+} in the material during adsorption: The coordination of Fe^{3+} is the dominant mechanism for TC adsorption,协同 with hydrogen bonding between CMCS and TC, while pore filling and cation-π interaction also participate.

The adsorbent demonstrated stable performance in cyclic adsorption experiments, maintaining an 85.20% TC removal rate after 8 cycles. Satisfactory adsorption results were achieved even under systems with different inorganic salt ion concentrations and in scenarios involving trace TC treatment in simulated aquaculture wastewater. Therefore, as an adsorbent, CMCS@Fe^{3+} exhibits great application potential for removing tetracycline antibiotic pollutants from composite wastewater.

References

[1] HAN Diangang, REN Tong, YANG Yuming, et al. Application and substitution of antibiotics in animal feeding[J]. Medycyna Weterynaryjna, 80(1): 6830-2024.

[2] ZHANG Chi, WEI Jiahua, HOU Xue, et al. Preparation of $CoFe_2O_4/MoS_2$ and its activation of PMS for tetracycline degradation[J]. Industrial Water Treatment, 2025, 45(6): 194-201.

[3] WANG Yuanyuan, SU Hong, LIU Deju, et al. Analysis on the global use of veterinary antibiotics from 2018 to 2020[J]. China Animal Health Inspection, 2022, 39(12): 72-77.

[4] DI CERBO A, PEZZUTO F, GUIDETTI G, et al. Tetracyclines: Insights and updates of their use in human and animal pathology and their potential toxicity[J]. The Open Biochemistry Journal, 2019, 13(1): 1-12.

[5] AMANGELSIN Y, SEMENOVA Y, DADAR M, et al. The impact of tetracycline pollution on the aquatic environment and removal strategies[J]. Antibiotics, 2023, 12(3): 440.

[6] WANG Fanjin, WANG Ziyi, ZHAO Yue, et al. Performance of traditional and emerging water-treatment technologies in the removal of tetracycline antibiotics[J]. Catalysts, 2024, 14(4): 269.

[7] GOPAL G, ALEX S A, CHANDRASEKARAN N, et al. A review on tetracycline removal from aqueous systems by advanced treatment techniques[J]. RSC Advances, 2020, 10(45): 27081-27095.

[8] RAI S, POKHREL S, UDASH P, et al. Chitin and chitosan from shellfish waste and their applications in agriculture and biotechnology industries[J]. Critical Reviews in Biotechnology, 2025, 45(7): 1508-1526.

[9] PISHEVAR A, KHANCHOUPAN M, AFRADI A, et al. Recent developments in chitosan-based adsorbents for tetracycline removal: A mini-review[J]. Synthesis and Sintering, 2025, 5(1): 41-51.

[10] KOU S, PETERS L M, MUCALO M R. Chitosan: A review of molecular structure, bioactivities and interactions with the human body and micro-organisms[J]. Carbohydrate Polymers, 2022, 282: 119132.

[11] JIMENEZ-GOMEZ C P, CECILIA J A. Chitosan: A natural biopolymer with a wide and varied range of applications[J]. Molecules, 2020, 25(17): 3981.

[12] KALLIOLA S, REPO E, SRIVASTAVA V, et al. Carboxymethyl chitosan and its hydrophobically modified derivative as pH-switchable emulsifiers[J]. Langmuir, 2018, 34(8): 2800-2806.

[13] KLOSINSKA K, WACHL A, GIREK-BAK M K, et al. Biocompatibility and mechanical properties of carboxymethyl chitosan hydrogels[J]. Polymers, 2022, 15(1): 144.

[14] LIU Huadong, XU Haoxuan, LI Hewei. Detection of Fe^{3+} and Hg^{2+} ions by using high fluorescent carbon dots doped with S and N as fluorescence probes[J]. Journal of Fluorescence, 2022, 32(3): 1089-1098.

[15] ZHAO Youjun, YU Lixin, DENG Yakun, et al. Highly stable N-doped carbon dots as the sensitive probe for the detection of Fe^{3+}[J]. Current Applied Physics, 2023, 50: 168-175.

[16] TIE Jianfei, LIU Hongchen, LV Jingchun, et al. Multi-responsive, self-healing and adhesive PVA based hydrogels induced by the ultrafast complexation of Fe^{3+} ions[J]. Soft Matter, 2019, 15(37): 7404-7411.

[17] WU Shang, LIU Jutao, FU Shuaishuai, et al. A novel acylhydrazone-based self-assembled supramolecular gel for ultrasensitive alternating fluorescence detection of Fe^{3+} and $H_2PO_4^-$[J]. New Journal of Chemistry, 2023, 47(28): 13152-13159.

[18] CAO Jinfeng, WU Ping, CHENG Qianqian, et al. Ultrafast fabrication of self-healing and injectable carboxymethyl chitosan hydrogel dressing for wound healing[J]. ACS Applied Materials & Interfaces, 2021, 13(20): 24095-24105.

[19] ZHOU Tianyi, ZHOU Haiyan, WANG Fei, et al. An injectable carboxymethyl chitosan hydrogel scaffold formed via coordination bond for antibacterial and osteogenesis in osteomyelitis[J]. Carbohydrate Polymers, 2024, 324: 121466.

[20] COTTON S A. Iron(III) chloride and its coordination chemistry[J]. Journal of Coordination Chemistry, 2018, 71(21): 3415-3443.

[21] GOSWAMI A, PENA-TORRES A, JONSSON E O, et al. Evidence of sharp transitions between octahedral and capped trigonal prism states of the solvation shell of the aqueous Fe^{3+} ion[J]. The Journal of Physical Chemistry Letters, 2024, 15(17): 4523-4530.

[22] HOU H, BAO Z, GAN X, et al. Probing conformation change and binding mode of metal ion-carboxyl coordination complex through resonant surface-enhanced Raman spectroscopy and density functional theory[J]. The Journal of Physical Chemistry Letters, 2019, 10(16): 4692-4698.

[23] TROTT O, OLSON A J. AutoDock Vina: Improving the speed and accuracy of docking with a new scoring function, efficient optimization, and multithreading[J]. Journal of Computational Chemistry, 2010, 31(2): 455-461.

[24] LI Ruchun, HU Zhaoxia, SHAO Xiaofeng, et al. Large scale synthesis of NiCo layered double hydroxides for

superior asymmetric electrochemical capacitor[J]. Scientific Reports, 2016, 6: 18737.
[25] LI Zhenghao, JIANG Hua, WANG Xipeng, et al. Effect of pH on adsorption of tetracycline antibiotics on graphene oxide[J]. International Journal of Environmental Research and Public Health, 2023, 20(3): 2448.
[26] LIAO Xinyi, CHEN Chen, LIANG Zhijie, et al. Selective adsorption of antibiotics on manganese oxide-loaded biochar and mechanism based on quantitative structure-property relationship model[J]. Bioresource Technology, 2023, 367: 128262.
[27] MASOUD A M, MUBARK A E, TAHA M H, et al. Nanostructured layered double hydroxide (NLDH)-Zn/Al-based materials: Strategy to improve performance for zirconium sorption from acidic sulfate solution[J]. RSC Advances, 2024, 14(39): 28455-28468.
[28] YU Fei, MA Jie, HAN Sheng. Adsorption of tetracycline from aqueous solutions onto multi-walled carbon nanotubes with different oxygen contents[J]. Scientific Reports, 2014, 4: 5326.
[29] NIU Yuzhong, LIU Huanhuan, QU Rongjun, et al. Preparation and characterization of thiourea-containing silica gel hybrid materials for Hg(II) adsorption[J]. Industrial & Engineering Chemistry Research, 2015, 54(5): 1656-1664.
[30] ZHENG Minghao, WU Panwang, LI Liqing, et al. Adsorption/desorption behavior of ciprofloxacin on aged biodegradable plastic PLA under different exposure conditions[J]. Journal of Environmental Chemical Engineering, 2023, 11(1): 109256.
[31] SHI Qiyu, WANG Wangbo, ZHANG Hongmin, et al. Porous biochar derived from walnut shell as an efficient adsorbent for tetracycline removal[J]. Bioresource Technology, 2023, 383: 129213.
[32] ZHAO Rui, MA Tingting, ZHAO Shuai, et al. Uniform and stable immobilization of metal-organic frameworks into chitosan matrix for enhanced tetracycline removal from water[J]. Chemical Engineering Journal, 2020, 382: 122893.
[33] DA SILVA BRUCKMANN F, SCHNORR C E, DA ROSA SALLES T, et al. Highly efficient adsorption of tetracycline using chitosan-based magnetic adsorbent[J]. Polymers, 2022, 14(22): 4854.
[34] LIN Jiayang, LIU Yue, HU Shen, et al. Ultra-fast adsorption of four typical pollutants using magnetically separable ethanolamine-functionalized graphene[J]. Separation and Purification Technology, 2021, 271: 118862.
[35] YANG Jing, DU Yu, LI Wenpeng, et al. Iron oxide/alginate hydrogel composites for removal of tetracycline via adsorption-coupled Fenton-like reaction[J]. Materials Chemistry and Physics, 2024, 315: 129034.
[36] AL-SALIHI S, FIDALGO M M, XING Yangchuan. Fast removal of tetracycline from aqueous solution by aluminosilicate zeolite nanoparticles with high adsorption capacity[J]. ACS ES&T Water, 2023, 3(3): 838-847.
[37] KURCZEWSKA J, CEGLOWSKI M. Alginate vs chitosan composites loaded with halloysite/molecularly imprinted polymer hybrids for tetracycline removal: Comparative studies of adsorption behaviour[J]. International Journal of Biological Macromolecules, 2025, 307: 142000.
[38] CHANG P H, MUKHOPADHYAY R, SARKAR B, et al. Insight and mechanisms of tetracycline adsorption on sodium alginate/montmorillonite composite beads[J]. Applied Clay Science, 2023, 245: 107127.
[39] XU Wencui, ZHONG Lubin, SHAO Zaidong, et al. Rational design of pore structures for carbon aerogels to significantly increase adsorption of tetracycline from water using batch and fixed-bed operation[J]. Environmental Science: Nano, 2021, 8(11): 3250-3261.
[40] MENG Yang, CHEN Xu, AI Dan, et al. Sulfur-doped zero-valent iron supported on biochar for tetracycline adsorption and removal[J]. Journal of Cleaner Production, 2022, 379: 134769.
[41] LI Yanjing, JIANG Qiushi, ZHANG Yuhan, et al. Preparation of nano-biochar by two-step method and study on the adsorption of tetracycline hydrochloride[J/OL]. Industrial Water Treatment, 2025: 1-17. (2025-08-04).
[42] WEI Zhengwen, MA Xuedong, ZHANG Yaoyao, et al. High-efficiency adsorption of phenanthrene by Fe_3O_4-SiO_2-dimethoxydiphenylsilane nanocomposite: Experimental and theoretical study[J]. Journal of Hazardous Materials, 2022, 422: 126948.
[43] ZHANG Youming, LI Yongfu, ZHONG Kaipeng, et al. A novel pillar[5]arene-based supramolecular organic framework gel to achieve an ultrasensitive response by introducing the competition of cation-π and π-π interactions[J]. Soft Matter, 2018, 14(18): 3624-3631.
[44] SHAHNAWAZ KHAN M, KHALID M, SHAHID M. Engineered Fe_3 triangle for the rapid and selective removal of aromatic cationic pollutants: Complexity is not a necessity[J]. RSC Advances, 2021, 11(5): 2630-2642.